

Pulse-power integrated-decay technique for the measurement of thermal conductivity

Nachiket M Kharalkar¹, Linda J Hayes² and Jonathan W Valvano¹

¹ Department of Electrical and Computer Engineering, The University of Texas at Austin,

1 University Station C0803, Austin, TX 78712, USA

² Department of Aerospace Engineering and Engineering Mechanics, The University of Texas at Austin,

1 University Station C0600, Austin, TX 78712, USA

E-mail: kharalkar@ieee.org

Received 5 December 2007, in final form 5 May 2008

Published 12 June 2008

Online at stacks.iop.org/MST/19/075104

Abstract

A pulse-power integrated-decay technique for the measurement of thermal conductivity of biological tissues is presented. A self-heated thermistor probe is used to deliver heat and also to measure the temperature response. Three-dimensional finite element analyses are used in this paper to design and optimize the technique. The thermal conductivity measurements from the computer simulations were in close accordance with the experimental data. An empirical calibration process, performed in glycerol and agar-gelled water, provides accurate thermal conductivity measurements. An accuracy analysis evaluated multiple experimental protocols using three solutions of known thermal properties. The results indicate that the thermal decay technique protocol had better accuracy than the constant temperature heating techniques.

In vitro measurements demonstrate the variability of tissue thermal conductivity, and the need to perform direct measurements for tissues of interest. The factors that may introduce error in the experimental data are (i) poor thermal/physical contact between the thermistor probe and tissue sample, (ii) water loss from tissue during the course of experimentation and (iii) temperature stability.

Keywords: 3D finite element modeling, thermal conductivity, instrumentation, self-heated thermistor, bioheat transfer

(Some figures in this article are in colour only in the electronic version)

Nomenclature

C	specific heat ($\text{J kg}^{-1} \text{K}^{-1}$)
ρ	density (kg m^{-3})
F	blood flow (ml s^{-1})
w	perfusion ($\text{ml s}^{-1} \text{ml}^{-1}$)
k	thermal conductivity ($\text{W m}^{-1} \text{K}^{-1}$)
T	temperature (K)
P	total thermistor electrical power (W)
t	time (s)
ΔT	volume average thermistor temperature rise (K)
Q	volumetric heat generation rate (W m^{-3})
r_t	radius of the thermistor (m)

Subscripts

h	heat mode
s	sense mode
eff	effective (conductivity and perfusion)

1. Introduction

The ultimate goal of this paper is to present a pulse-power integrated thermal decay technique for the measurement of thermal conductivity of biological tissues, using a self-heated thermistor. This paper presents thermal data comparing different techniques for the measurement of

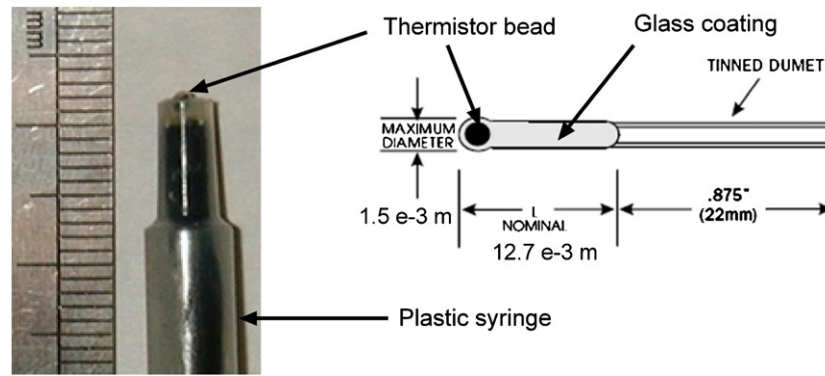


Figure 1. P60 thermistor probe.

thermal conductivity. Three-dimensional finite element analyses were used to design and optimize the technique. Accuracy was determined experimentally by operating in materials of known properties. The instrumentation system was used to perform thermal conductivity measurements on biological tissue *in vitro*.

1.1. Significance

The study of heat-transfer mechanisms occurring in biomaterials is important because many biological measurements are extremely sensitive to temperature. Accurate values of tissue thermal properties are vital to predict these heat-transfer mechanisms. For example, the estimation of the extent of injury due to skin burn using bioheat transfer models requires accurate thermal properties of underlying skin layers [1–3]. Precise measurement of tissue thermal properties is necessary for multilayered tissue characterization [4]. Accurate measurement of tissue thermal properties is also necessary for tumor detection using magnetic resonance and focused ultrasound heating [5].

2. Background

Self-heated thermistors have been widely used for the measurement of tissue thermal properties [6–12]. Normally thermistors are used to measure temperature, but in the self-heated thermistor technique they are also used to heat the tissue samples, in order to measure the tissue thermal properties. The thermistor can be heated using different heating protocols. For example, Valvano *et al* have measured the thermal properties of biomaterials using the constant temperature and sinusoidal heating techniques [6–8, 10, 13–16]. Valvano *et al* have used the sinusoidal heating technique to measure the intrinsic thermal conductivity of tissue in the presence of blood flow. Liu *et al* have proposed a non-invasive sinusoidal heating technique to measure tissue perfusion [12]. Liu *et al* have used a low frequency (period = 0.02–1 s) sinusoidal heating pulse to measure the tissue perfusion non-invasively. They have used the phase shift between heat flux and temperature response to predict the tissue perfusion. However, for a low perfusion $0.0005 \text{ ml s}^{-1} \text{ ml}^{-1}$, the time for the phase shift to reach the final constant value is about 4500 s.

A thermal pulse decay technique to measure thermal conductivity and blood perfusion was proposed by Chen *et al* and further enhanced by Diederich *et al* [9, 17–19]. In the thermal pulse decay technique, Chen *et al* heat the thermistor for about 3 s and then monitor the temperature decay for the next 3–11 s after the heat pulse is turned off. The thermal properties are calculated by fitting the local temperature decay to that predicted by a theoretical model. As compared to the constant temperature heating technique, this technique has an advantage of larger measuring volume and faster measurements. However, in order to measure the thermal conductivity of the specimen using the pulse-decay technique, prior knowledge of specimen density and specific heat is required [20].

Hayes *et al* have used a two-dimensional axisymmetric finite element method to model the three-dimensional self-heated thermistor system [21, 22]. They have used finite element analysis to calculate the steady-state temperature profiles generated by thermistor beads with realistic geometry and heating patterns. They successfully validated the experimental technique using finite element analysis.

3. Methods

3.1. Thermistor-probe design

A number of factors must be considered while designing the thermistor probe. A larger thermistor size has the advantage of having an effective volume of measurement. Finite element studies have shown that the effective volume of measurement in the tissue extends to 5–10 thermistor radii [7, 21]. A smaller thermistor size has the advantage of a faster response time. As a compromise of these factors, a glass encapsulated thermistor P60DA102K by Thermometrics, with a radius of about $7.5 \times 10^{-4} \text{ m}$ was used in this study. A schematic of the thermistor probe used to make surface measurements is presented as figure 1. The thermistor has a nominal resistance of 1 k Ω at 298.15 K, and a thermal time constant of 0.3 s when plunged into water. The actual probe was constructed by inserting this thermistor inside a plastic syringe, such that about $5 \times 10^{-4} \text{ m}$ of the thermistor bead protruded from the syringe and the rest of the syringe was filled with silicone for thermal and electrical insulation, as shown in figure 1.

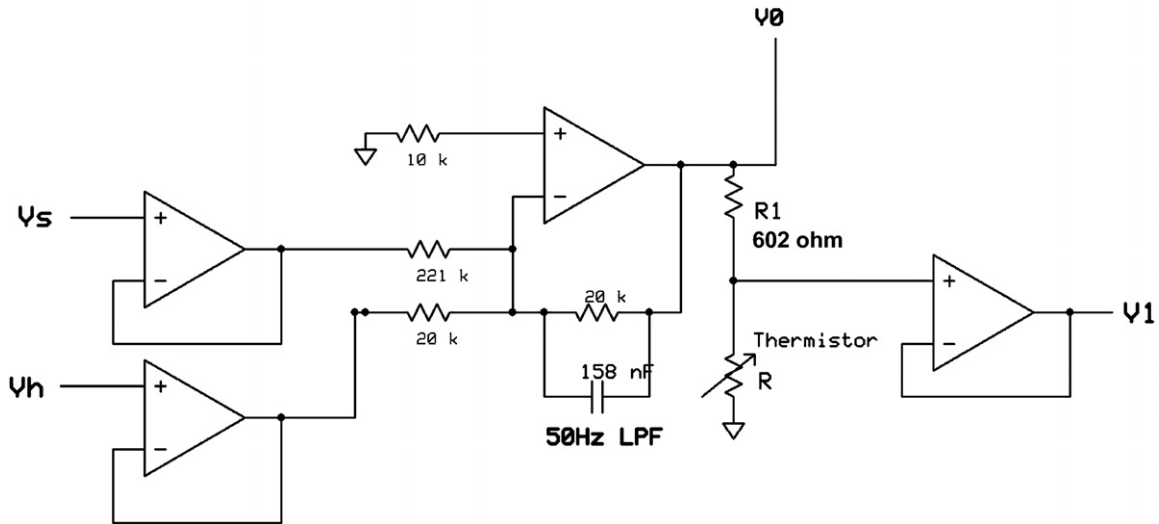


Figure 2. Circuit diagram.

3.2. Instrumentation

The thermistor was connected in series with a fixed value resistor (R_1) and the other end of the thermistor (R) was grounded, as shown in figure 2. The National Instruments M-series data acquisition board PCI-6221 (16-bit, 250 kHz) was used to output and acquire the analog voltages. The analog outputs and inputs from the data acquisition board were buffered using the operational amplifiers. A LabVIEW™ based data acquisition system was designed that outputted -2.98 V to the V_s channel and 0 V to the V_h channel during the temperature sensing phase, causing V_0 to be about 0.269 V. During the heating phase, depending on the heating protocol -3.6 or -10 V was outputted to the V_h channel while 0 V was outputted to the V_s channel. -3.6 V was chosen since that gave maximum temperature rise of about 1.5 K from the baseline, which would cause no tissue damage due to heating. -10 V was chosen, to test the performance at a higher temperature rise. The voltages V_0 and V_1 were continuously recorded using the two 16-bit analog input channels at 80 kHz and then digitally low pass filtered at 44 Hz. The channels were over-sampled at 80 kHz and then averaged inside the LabVIEW software for a better signal-to-noise ratio.

The transient thermistor resistance $R(t)$ was calculated using equation (1):

$$R(t) = \frac{V_1(t)R_1}{V_0(t) - V_1(t)}. \quad (1)$$

The natural log function was used to calculate the transient thermistor temperature $T(t)$ from the thermistor resistance $R(t)$ by using equation (2). Equation (2) showed better accuracy than the three-term (H_0 , H_1 and H_3) equation used by Valvano et al [6–8]:

$$T(t) = 1/\{H_0 + H_1 \ln R(t) + H_2(\ln R(t))^2 + H_3(\ln R(t))^3 + H_4(\ln R(t))^4\} - 273.15. \quad (2)$$

$T(t)$ was the temperature in degree Celsius and H_0 , H_1 , H_2 , H_3 and H_4 were calibration coefficients. The transient

power dissipated across the thermistor was calculated using equation (3):

$$P(t) = \frac{V_1(t)^2}{R(t)}. \quad (3)$$

V_s was set to -2.98 V and V_h to 0 V, during the temperature measurement phase. The initial baseline temperature T_0 was recorded using equations (1) and (2).

3.3. Constant voltage heating protocol

For the ‘3.6 V 3 s heat’ protocol the thermistor was heated for 3 s by making V_h equal to -3.6 V and V_s equal to 0 V. During the heating phase the thermistor temperature and the power dissipated across the thermistor were continuously recorded using equations (1)–(3). The temperature rise $\Delta T(t)$ was calculated using equation (4):

$$\Delta T(t) = T(t) - T_0. \quad (4)$$

The applied power P was nearly constant during the 3 s heating phase while the temperature rise $\Delta T(t)$ varied considerably. A plot of $P(t)/\Delta T(t)$ versus $t^{-1/2}$ was made. D and E were calculated by fitting 1–3 s heating data to equation (5) using linear regression. The first 1 s of heating data was

$$\frac{P(t)}{\Delta T(t)} = Dt^{-1/2} + E \quad (5)$$

skipped, in order for the system to stabilize. Equation (6) was used to calculate the thermal conductivity [4, 6–8, 13]. In equation (6), a_1 and a_2 are empirical coefficients defined by the thermistor size and properties:

$$k = \frac{1}{\frac{a_1}{E} + a_2}. \quad (6)$$

For the ‘10 V 3 s heat’ protocol the thermistor was heated for 3 s by making V_h equal to -10 V and V_s equal to 0 V. Similarly for the ‘3.6 V 9 s heat’ protocol the thermistor was heated for 9 s by making V_h equal to -3.6 V and V_s equal to 0 V. Also for the ‘3.6 V 9 s heat’ protocol, D and E were calculated by fitting 1 to 9 s of heating data to equation (5) using linear regression.

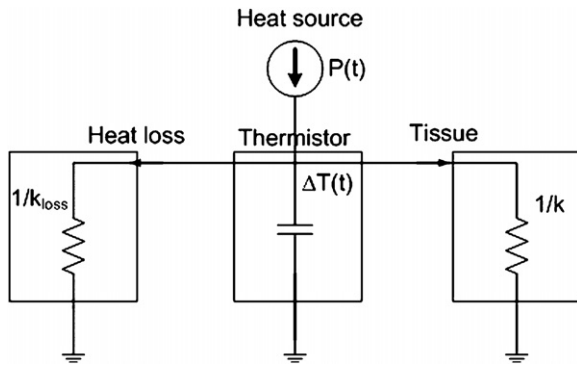


Figure 3. Heat flow model.

3.4. Cooling integral protocol

For the ‘3.6 V 3 s cool area’ protocol the thermistor was heated for 3 s by making V_h equal to -3.6 V and V_s equal to 0 V. Following the heating phase, the thermistor was put back into measurement mode, and the temperature decay was measured for 3 more seconds. The temperature rise $\Delta T(t)$ was calculated using equation (4). A plot of $\Delta T(t)$ versus t was made. Similar to the thermal dilution technique the energy balance equation can be modeled as shown in figure 3 and expressed as shown in equation (7):

$$E_{in} + E_{tissue} + E_{loss} = 0. \quad (7)$$

As shown in equation (8), input energy (positive) is related to the delivered power. In equation (8) t_h is the time of heating ($t_h = 3$ s for ‘3.6 V 3 s heat’, ‘10 V 3 s heat’, ‘10 V 3 s cool area’ and ‘3.6 V 3 s cool area’ protocols; $t_h = 9$ s for ‘3.6 V 9 s heat’ and ‘3.6 V 9 s cool area’ protocols):

$$E_{in} = \int_0^{t_h} P(t) dt. \quad (8)$$

The conductive loss depends on an area (A_{loss}), characteristic length (r_{loss}) and the conductivity (k_{loss}) of all thermal pathways not into the tissue (thermistor lead wires are the major component) as shown in equation (9):

$$E_{loss} \approx -\frac{A_{loss} k_{loss}}{r_{loss}} \int_{t-t_h}^{t-t_h+2.69} \Delta T(t) dt \quad (9)$$

The cooling area was calculated from $t = t - t_h$ to $t = t - t_h + 2.69$. It was calculated for 2.69 s since within 2.69 s the temperature dropped (about 85%) close to the initial baseline temperature.

The energy into the tissue also depends on a semispherical area of the thermistor ($2\pi r_t^2$), the characteristic length r_t and the tissue thermal conductivity, as shown in equation (10):

$$E_{tissue} = \int (\text{Heat flow}) dt \approx -\frac{2\pi r_t^2 k}{r_t} \int_{t-t_h}^{t-t_h+2.69} \Delta T(t) dt. \quad (10)$$

Substituting equations (8)–(10) in equation (7), we obtain equation (11):

$$\frac{1}{k} = 2\pi r_t \frac{\int_{t-t_h}^{t-t_h+2.69} \Delta T(t) dt}{\int_0^{t_h} P(t) dt} - \frac{2\pi r_t r_{loss}}{A_{loss} k_{loss}}. \quad (11)$$

$P(t)$ is almost constant during the heating phase and hence E_{in} is almost constant in equation (8). Also A_{loss} , r_{loss} and k_{loss} can be assumed to be constant in equation (9), because these constants depend on thermistor size and the physical properties of the probe. Simplifying equation (11) thermal conductivity may be estimated by equation (12). The integral of $\Delta T(t)$ is calculated by finding area under curve for the cooling data:

$$k = \frac{1}{a_3 \frac{\int_{t-t_h}^{t-t_h+2.69} \Delta T(t) dt}{\int_0^{t_h} P(t) dt} - a_4} \quad (12)$$

where a_3 and a_4 are empirical coefficients representing properties of the thermistor probe. For the ‘10 V 3 s cool area’ protocol the thermistor was heated for 3 s by making V_h equal to -10 V and V_s equal to 0 V. Similarly, for the ‘3.6 V 9 s cool area’ protocol the thermistor was heated for 9 s by making V_h equal to -3.6 V and V_s equal to 0 V.

3.5. Perfusion dependence

Perfusion has a significant impact on heat transfer *in vivo*. Heat deposited locally into living tissue can transfer via conduction to surrounding tissues, or via convection with moving blood. The situation is complicated by the fact that perfusion affects temperature and temperature affects perfusion. The modeling of these interactions is beyond the scope of this paper. However, the self-heated thermistor technique described in this paper could be employed *in vivo* to measure the effective thermal conductivity (k_{eff}), which is a combination of both the conductive and convective components. Previous experimental studies with other self-heated thermistor techniques have shown a linear relationship between measured effective thermal conductivity and perfusion. Patel *et al* [8] placed a thermistor probe on the surface of a rat liver measuring k_{eff} as a function of flow. The liver flow ranged from 0 to 0.27 ml s⁻¹ causing a conductivity change from 0.58 to 0.64 W m⁻¹ K⁻¹. Patel obtained this relationship shown in equation (13):

$$k_{eff} = 0.579 + 0.252F \quad (13)$$

where F is the total flow in a rat liver (ml s⁻¹). Anderson *et al* [10] placed a thermistor probe inside a canine kidney measuring k_{eff} as a function of perfusion. The kidney perfusion ranged from 0 to 0.017 ml s⁻¹ ml⁻¹ causing a conductivity change from 0.56 to 0.63 W m⁻¹ K⁻¹. Anderson obtained the relationship shown in equation (14):

$$k_{eff} = 0.563 + 3.78w \quad (14)$$

where w is the perfusion in the canine kidney (ml s⁻¹ ml⁻¹). To accurately measure the perfusion, one would need a realistic model describing the thermal effects of perfusion and one would need careful calibration. However, to detect relative changes in perfusion, one could simply use this technique to measure the effective thermal conductivity.

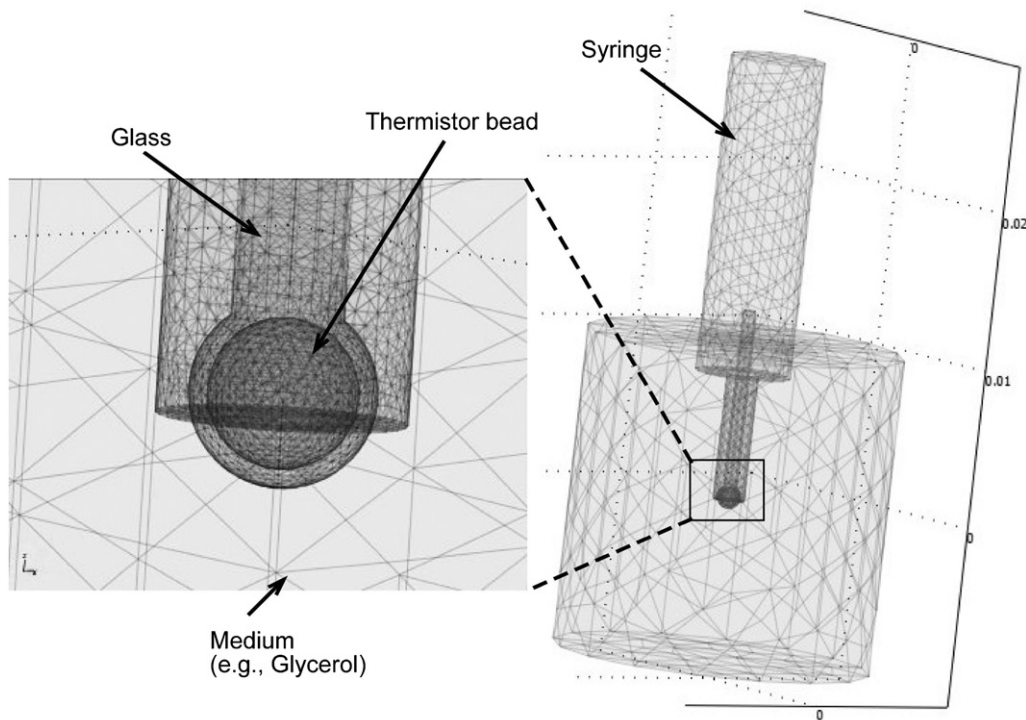


Figure 4. Finite element model.

4. Calibration procedures

4.1. Temperature calibration

In order to measure the temperature, the resistance versus temperature characteristics of the thermistor probe were required. The true temperature was measured by a quartz precision thermometer (Hewlett Packard, 2804A, Quartz thermometer, resolution = 0.0001 K, accuracy = 0.001 K). 13 calibration points were taken from temperature range of 308.65 K to 333.15 K (35.5 to 60 °C). The true temperature was noted using the quartz thermometer and the corresponding resistance of the thermistor was measured from LabVIEW™ software. A chi-squared nonlinear regression was used to calculate H_0 , H_1 , H_2 , H_3 and H_4 from the calibration data for the thermistor probe. The average accuracy determined by performing a second experiment with the same quartz thermometer was 0.009 K for this system.

4.2. Thermal conductivity calibration

In order to measure the thermal conductivity, the coefficients a_1 , a_2 , a_3 and a_4 in equations (6) and (12) had to be determined. Glycerol and 1% agar-gelled water were used as two liquids with known thermal properties to calculate these coefficients. The thermistor probe was immersed in both these liquids and kept in a temperature-controlled water bath maintained at 311.15 K (38 °C). The calibration was performed only after the probe and the liquid temperature had stabilized at 311.15 K.

Table 1. Thermal properties of materials used in this study.

Material	k (W m ⁻¹ K ⁻¹)	C (J kg ⁻¹ K ⁻¹)	ρ (kg m ⁻³)
Agar-gelled water	0.609	4180	997
Glass	1.380	703	2203
Glycerol	0.286	2427	1260
Thermistor bead	0.100	159	6300
90G:10A	0.305	2602	1186
68G:32A	0.358	2997	1081
47G:53A	0.422	3364	1031

5. Finite element analysis

Finite element analysis was performed using COMSOL Multiphysics™ 3.3a. Equation (15) was used to model the system. Equation (15) is the transient heat transfer equation. The 3D model shown in figure 4 was used to do the finite element analysis:

$$\rho C \frac{\partial T}{\partial t} + \nabla \cdot (-k \nabla T) = Q. \quad (15)$$

In equation (15), Q is the heat source term. Table 1 indicates the values of thermal properties of different materials modeled in figure 4. T_0 was assumed to be 311.15 K. The temperature ' T ' was recorded by taking the volume integral of the temperature over the thermistor bead.

6. Results

Water/glycerol mixtures were used to measure accuracy of the different thermal conductivity measurement protocols.

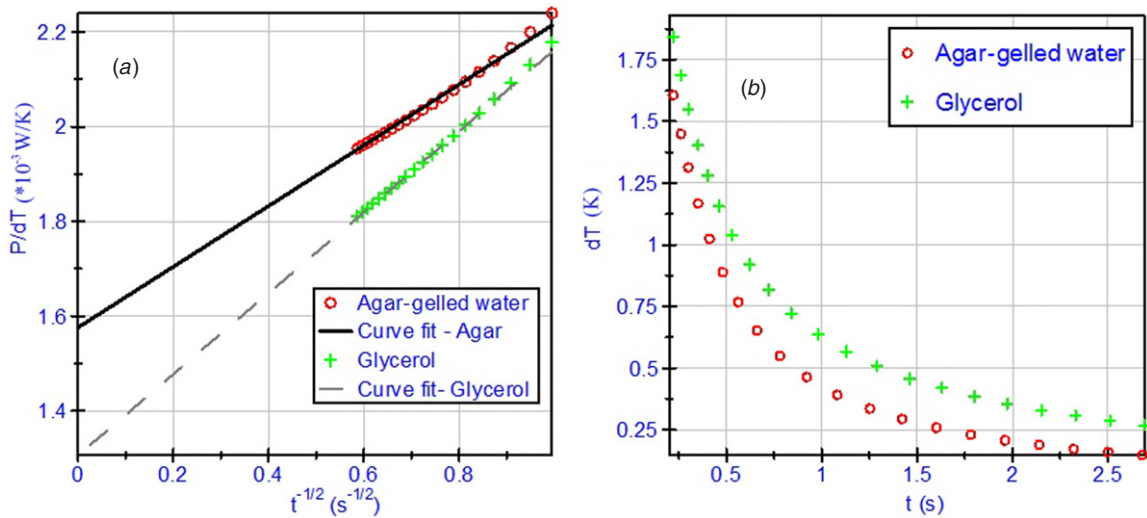


Figure 5. Finite element analysis ‘3.6 V 3 s heat and cool area’ protocols.

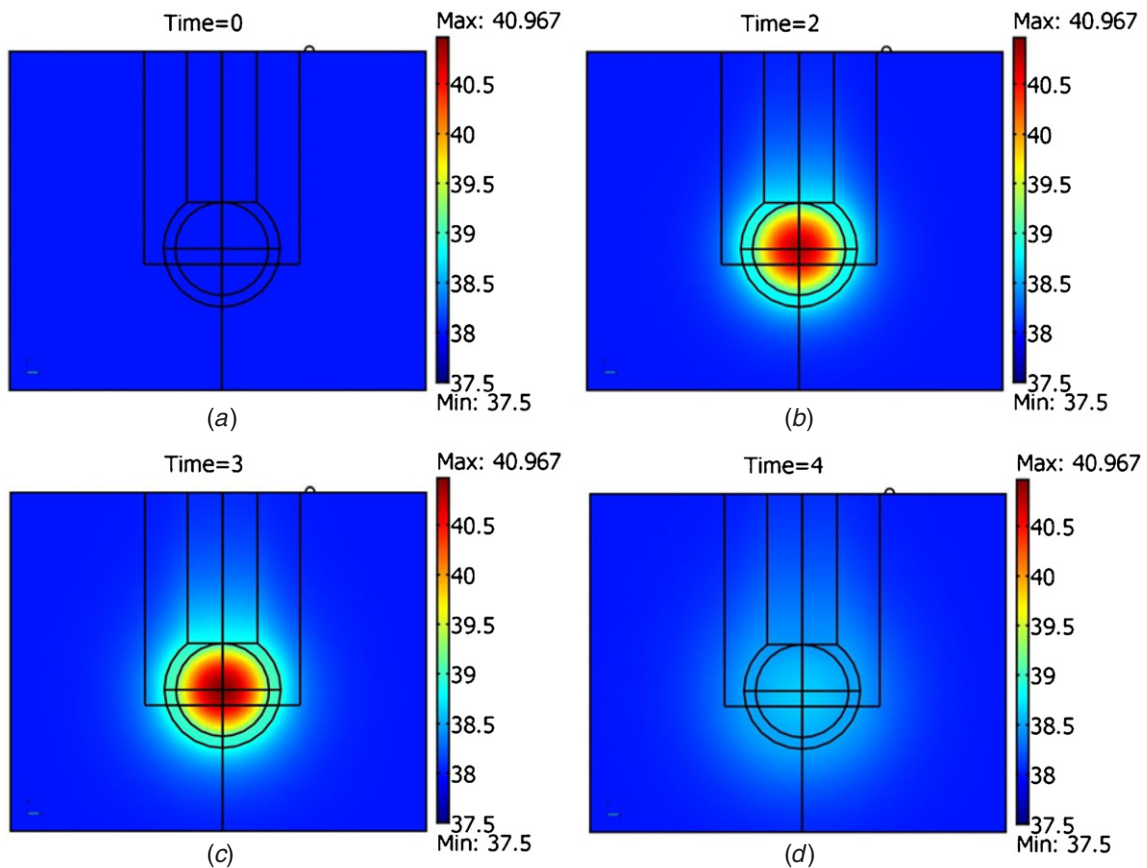


Figure 6. FEA simulation temperature profile obtained with glycerol.

The ‘90G:10A’ material in table 1 indicates approximately 90% glycerol and 10% agar-gelled water mixture. Similarly, the ‘68G:32A’ material was made with approximately 68% glycerol and 32% agar-gelled water, while ‘47G:53A’ was made with 47% glycerol and 53% agar-gelled water. The thermal conductivities of these mixtures were estimated from the mass fraction [23].

6.1. Finite element analysis data

The applied power P from the experimental analysis was $5.35 \times 10^{-3} \text{ W}$ for 3.6 V heating while $4.09 \times 10^{-2} \text{ W}$ for the 10 V heating protocol. The volumetric heat generation rate Q in equation (15) for 3.6 V heating protocol was $5.91 \times 10^6 \text{ W m}^{-3}$ and $4.522 \times 10^7 \text{ W m}^{-3}$ for the 10 V heating protocol. The experimental protocol was simulated using finite

Table 2. Summary of thermal conductivity as obtained from FEA.

Experiment protocol	Media	True k (W m ⁻¹ K ⁻¹)	k from FEA (W m ⁻¹ K ⁻¹)	% error in k	Average % error in k
3.6 V 3 s heat	90G:10A	0.305	0.302	0.9	1.6
	68G:32A	0.358	0.351	2.0	
	47G:53A	0.422	0.413	2.0	
10 V 3 s heat	90G:10A	0.305	0.302	0.9	1.6
	68G:32A	0.358	0.351	2.0	
	47G:53A	0.422	0.413	2.0	
3.6 V 9 s heat	90G:10A	0.305	0.303	0.7	1.4
	68G:32A	0.358	0.352	1.7	
	47G:53A	0.422	0.415	1.7	
3.6 V 3 s cool area	90G:10A	0.305	0.301	1.4	3.1
	68G:32A	0.358	0.345	3.6	
	47G:53A	0.422	0.404	4.1	
10 V 3 s cool area	90G:10A	0.305	0.301	1.4	3.1
	68G:32A	0.358	0.345	3.6	
	47G:53A	0.422	0.404	4.2	
3.6 V 9 s cool area	90G:10A	0.305	0.303	0.6	2.1
	68G:32A	0.358	0.349	2.7	
	47G:53A	0.422	0.409	3.0	

element modeling, and the temperature responses for different experimental conditions were recorded. Figure 5(a) shows a sample plot of $P/\Delta T$ versus $t^{-1/2}$ generated using the 3D finite element simulation of the probe in the agar-gelled water and glycerol, used in the '3.6 V 3 s heat' protocol. Figure 5(b) shows a sample plot of ΔT versus t , recorded using the 3D finite element simulation of the probe in the agar-gelled water and glycerol, used in the '3.6 V 3 s cool area' protocol.

Figure 6 shows the temperature distribution obtained from the finite element analysis of the probe in glycerol, using the '3.6 V 3 s heat' protocol. Figure 6(a) is the slice taken through the center of the 3D probe-glycerol system at time equal to 0 s. Similarly, figure 6(b) shows the temperature distribution at time equal to 2 s, figure 6(c) shows at 3 s and figure 6(d) shows at time equal to 4 s.

The probe was empirically calibrated (using the same method as experiments) by operating the probe in glycerol and then in agar-gelled water to determine the calibration coefficients a_1 , a_2 , a_3 and a_4 . The summary of the calibrated values of thermal conductivities as obtained from the finite element analysis is shown in table 2.

Figure 7 shows a comparison of true thermal conductivities and thermal conductivities of three mixtures, as obtained from finite element simulations using the different experimental protocols.

6.2. Experimental data from the water/glycerol mixtures

The thermistor probe was inserted into each individual mixture; the mixture-probe system was then placed in a temperature-controlled water bath. Thermal conductivity was measured seven times for each protocol at 311.15 K. The probe was empirically calibrated by operating the probe in glycerol and then in agar-gelled water to determine the calibration coefficients a_1 , a_2 , a_3 and a_4 . The calibrated values of the

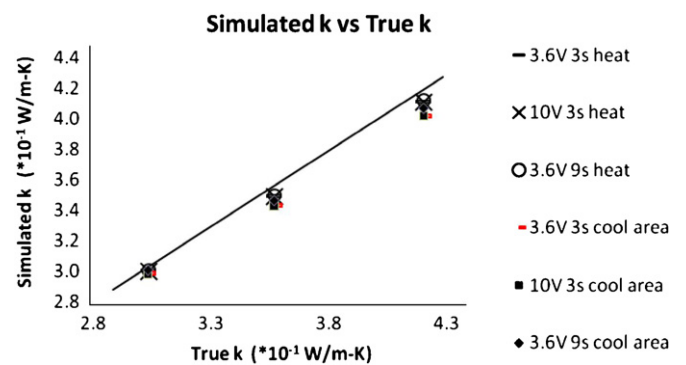


Figure 7. Simulated and true thermal conductivity comparison (line is ideal response).

thermal conductivity for all the experimental protocols have been summarized in table 3. Each thermal conductivity value in table 3 is the average of seven independent measurements.

Figure 8 shows the probe temperature and power variations with respect to time, as obtained from the experimental analysis using the '10 V 3 s heat' protocol on agar-gelled water, glycerol and different mixtures.

Figure 9 shows a comparison of true thermal conductivities and measured thermal conductivities of three mixtures, using the different experimental protocols. The '3.6 V 3 s cool area' protocol had the least error (1.2%) and may be reliably used for the thermal conductivity measurements.

6.3. Experimental data from the biological tissues

The instrument was used to measure thermal conductivity of biologic tissue *in vitro*. The 3.6 V 3 s heat and 3.6 V 3 s cool area protocols were used. The experiments were performed on fresh samples of Angus beef consisting of muscle and fatty tissue and also on the human tissues. All tissue samples were

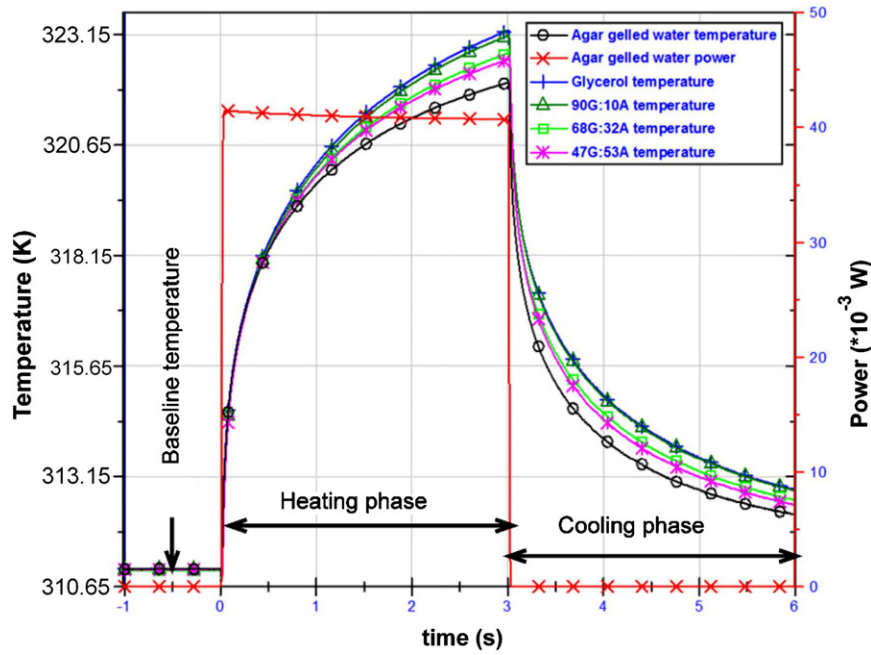


Figure 8. Experimental 10 V 3 s.

Table 3. Summary of thermal conductivity as obtained from experimental analysis.

Experiment protocol	Media	True k ($W m^{-1} K^{-1}$)	Average experimental k ($W m^{-1} K^{-1}$)	Standard deviation measured k ($W m^{-1} K^{-1}$)	% error in k	Average % error in k
3.6 V 3 s heat	90G:10A	0.305	0.296	0.001	2.9	3.2
	68G:32A	0.358	0.377	0.001	-5.3	
	47G:53A	0.422	0.428	0.001	-1.4	
10 V 3 s heat	90G:10A	0.305	0.295	0.002	3.4	2.5
	68G:32A	0.358	0.372	0.001	-3.7	
	47G:53A	0.422	0.420	0.003	0.5	
3.6 V 9 s heat	90G:10A	0.305	0.294	0.001	3.5	2.2
	68G:32A	0.358	0.366	0.001	-2.1	
	47G:53A	0.422	0.426	0.001	-1.0	
3.6 V 3 s cool area	90G:10A	0.305	0.299	0.001	2.0	1.2
	68G:32A	0.358	0.363	0.010	-1.2	
	47G:53A	0.422	0.420	0.006	0.4	
10 V 3 s cool area	90G:10A	0.305	0.291	0.002	4.6	2.8
	68G:32A	0.358	0.357	0.002	0.4	
	47G:53A	0.422	0.407	0.003	3.5	
3.6 V 9 s cool area	90G:10A	0.305	0.286	0.002	6.1	4.2
	68G:32A	0.358	0.347	0.003	3.2	
	47G:53A	0.422	0.408	0.003	3.2	

Table 4. *In vitro* thermal conductivity measurements of biological tissues.

Tissue source	Tissue type	'3.6 V 3s heat'				'3.6 V 3s cool area'	
		'3.6 V 3s heat' k ($W m^{-1} K^{-1}$)	Standard deviation in k ($W m^{-1} K^{-1}$)	'3.6 V 3s heat' k ($W m^{-1} K^{-1}$)	Standard deviation in k ($W m^{-1} K^{-1}$)	'3.6 V 3s cool area' k ($W m^{-1} K^{-1}$)	Standard deviation in k ($W m^{-1} K^{-1}$)
Bovine	Fat ($n = 5, m = 5$)	0.260	0.009	0.288	0.004		
Bovine	Muscle ($n = 3, m = 3$)	0.501	0.028	0.473	0.016		
Human	Aorta ($n = 3, m = 9$)	0.588	0.008	0.571	0.009		
Human	Carotid artery ($n = 2, m = 6$)	0.532	0.018	0.543	0.015		
Human	Femoral artery ($n = 2, m = 6$)	0.537	0.021	0.531	0.020		
Human	Aortic valve ($n = 1, m = 3$)	0.336	0.001	0.337	0.003		

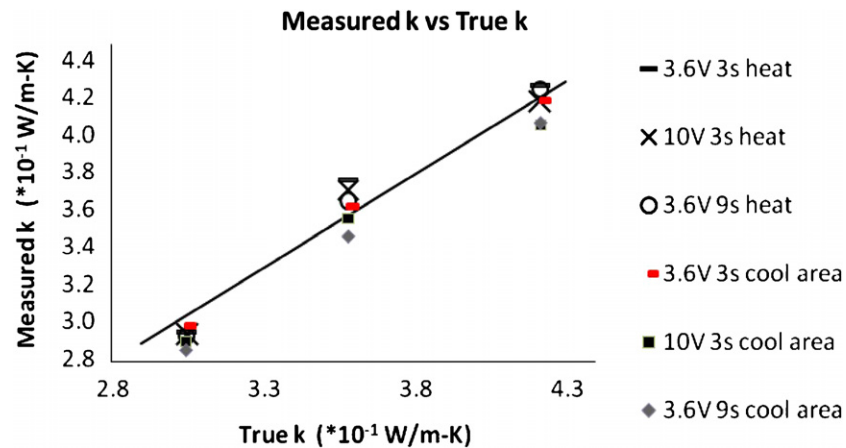


Figure 9. Measured and true thermal conductivity comparison (line is ideal response).

placed on cotton gauze soaked in saline solution (isotonic sterile aqueous solution containing a borate buffer system and sodium chloride) in order to prevent water loss from the tissue during the experiments. During the measurements, the tissue samples were kept in a water-tight chamber immersed in a temperature-controlled water bath, maintained at 311.15 K (38 °C). The thermistor probe was placed on the samples, and the measurements were taken only after the initial baseline temperature measured by the thermistor was stable (less than 0.03 K s^{-1}). External weights were used to hold the thermistor probe on the tissue, exerting a pressure of about 1500 kg m^{-2} , which was constant for all the samples. Experimental results have been shown in table 4. In table 4 n is the number of tissue samples and m is the total number of measurements.

7. Conclusions

A pulse-power integrated-decay technique for the measurement of thermal conductivity of biological tissues, using the self-heated thermistor has been successfully developed and tested. The experimental analysis shows that the '3.6 V 3 s cool area' protocol has better accuracy than the other protocols. A lower heating power ($5.35 \times 10^{-3} \text{ W}$) means a lower temperature rise in the tissue and hence no tissue damage. Also, a shorter heating time means the temperature will return to baseline value more quickly and hence more measurements can be performed in fixed amount of time. As seen from figures 7 and 9, all the techniques have the ability to measure thermal conductivity with about 4.2% accuracy. Thermal conductivity experiments and 3D finite element computer simulations exhibit the same behavior; in particular both the equations (6) and (12) can be used to measure the tissue thermal conductivity. Two advantages of the integrated-decay technique are that it is derived from fundamental principles (figure 3 and equation (11)), and the results are calculated from both, heating and cooling data. *In vitro* measurements demonstrate the variability of tissue thermal conductivity, and the need to perform direct measurements for tissues of interest. As seen from table 4, the integrated-decay technique can be used to measure tissue thermal conductivity, and measurements clearly reflect the

tissue composition. The thermal conductivity was low for tissues having higher lipid or fat content and high for fibrous tissues and the tissues containing more water. Proper thermal contact between the thermistor probe and tissue sample is extremely important for this method to work successfully and is the main factor that may introduce errors in the experiment.

Acknowledgments

The authors would like to thank Robin Tsang for his help in analog and digital signal processing.

References

- [1] Torvi D A and Dale J D 1994 A finite element model of skin subjected to a flash fire *J. Biomech. Eng.* **116** 250–5
- [2] Liu J, Chen X and Xu L X 1999 New thermal wave aspects on burn evaluation of skin subjected to instantaneous heating *IEEE Trans. Biomed. Eng.* **46** 420–8
- [3] Diller K R and Hayes L J 1991 Analysis of tissue injury by burning: comparison of in situ and skin flap models *Int. J. Heat Mass Transf.* **34** 1393–406
- [4] Kharalkar N M and Valvano J W 2006 Finite element analysis and experimental verification of multilayered tissue characterization using the thermal technique *Conf. Proc. IEEE Eng. Med. Biol. Soc.* vol 1 pp 3182–5
- [5] Cheng H L and Plewes D B 2002 Tissue thermal conductivity by magnetic resonance thermometry and focused ultrasound heating *J. Magn. Reson. Imag.* **16** 598–609
- [6] Valvano J W and Chitsabesan B 1987 Thermal conductivity and diffusivity of arterial wall and atherosclerotic plaque *Lasers Life Sci.* **1** 11
- [7] Valvano J W, Cochran J R and Diller K R 1985 Thermal conductivity and diffusivity of biomaterials measured with self-heated thermistors *Int. J. Thermophys.* **6** 301–11
- [8] Patel P A, Valvano J W, Pearce J A, Prah S A and Denham C R 1987 A self-heated thermistor technique to measure effective thermal properties from the tissue surface *J. Biomech. Eng.* **109** 330–5
- [9] Chen M M, Holmes K R and Rupinskis V 1981 Pulse-decay method for measuring the thermal conductivity of living tissues *J. Biomech. Eng.* **103** 253–60

- [10] Anderson G T, Valvano J W and Santos R R 1992 Self-heated thermistor measurements of perfusion *IEEE Trans. Biomed. Eng.* **39** 877–85
- [11] Bowman H F and Balasubramaniam T A 1976 A new technique utilizing thermistor probes for the measurement of thermal properties of biomaterials *Cryobiology* **13** 572–80
- [12] Liu J, Zhou Y X and Deng Z S 2002 Sinusoidal heating method to noninvasively measure tissue perfusion *IEEE Trans. Biomed. Eng.* **49** 867–77
- [13] Valvano J W, Allen J T and Bowman H F 1984 The simultaneous measurement of thermal conductivity, thermal diffusivity, and perfusion in small volumes of tissue *J. Biomech. Eng.* **106** 192–7
- [14] Bhavaraju N C, Cao H, Yuan D Y, Valvano J W and Webster J G 2001 Measurement of directional thermal properties of biomaterials *IEEE Trans. Biomed. Eng.* **48** 261–7
- [15] Bhavaraju N C and Valvano J W 1999 Thermophysical properties of swine myocardium *Int. J. Thermophys.* **20** 665–76
- [16] Anderson G T and Valvano J W 1994 A small artery heat transfer model for self-heated thermistor measurements of perfusion in the kidney cortex *J. Biomech. Eng.* **116** 71–8
- [17] Diederich C J, Clegg S and Roemer R B 1989 A spherical source model for the thermal pulse decay method of measuring blood perfusion: a sensitivity analysis *J. Biomech. Eng.* **111** 55–61
- [18] Arkin H, Holmes K R and Chen M M 1989 A technique for measuring the thermal conductivity and evaluating the ‘apparent conductivity’ concept in biomaterials *J. Biomech. Eng.* **111** 276–82
- [19] Arkin H, Holmes K R and Chen M M 1986 A sensitivity analysis of the Thermal Pulse Decay method for measurement of local tissue conductivity and blood perfusion *J. Biomech. Eng.* **108** 54–8
- [20] Chen Y-J 1992 Comparison between constant delta-T and Chen-Holmes pulse-decay methods for measurement of thermal conductivity *Master’s Report* The University of Texas at Austin (Dec. chapter 6:64–8)
- [21] Hayes L J and Valvano J W 1985 Steady-state analysis of self-heated thermistors using finite elements *J. Biomech. Eng.* **107** 77–80
- [22] Hayes L J and Diller K R 1983 A finite element model for phase change heat transfer in a composite tissue with blood perfusion *ISA Trans.* **22** 33–7
- [23] Diller K R, Valvano J W and Pearce J A 2000 Bioheat transfer *The CRC Handbook of Thermal Engineering* ed F Kreith (Boca Raton, FL: CRC Press) pp 4–120